frontiers | Frontiers in Physics

TYPE Original Research
PUBLISHED 16 May 2023
DOI 10.3389/fphy.2023.1163299

OPEN ACCESS

EDITED BY
Rosario Gianluca Pizzone,
Laboratori Nazionali del Sud (INFN), Italy

REVIEWED BY
Gábor Kiss,
Institute for Nuclear Research (MTA), Hungary
Roberto Linares,
Fluminense Federal University, Brazil

*CORRESPONDENCE
K. Y. Chae,
kchae@skku.edu

RECEIVED 10 February 2023
ACCEPTED 02 May 2023
PUBLISHED 16 May 2023

CITATION
Cha SM, Chae KY, Abe K, Bae S, Binh DN, Choi SH, Duy NN, Ge Z, Hahn KI, Hayakawa S, Hong B, Iwasa N, Kahl D, Khiem LH, Kim A, Kim D, Kim EJ, Kim GW, Kim MJ, Kwak K, Kwag MS, Lee EJ, Lim SI, Moon B, Moon JY, Park SY, Phong VH, Shimizu H, Yamaguchi H and Yang L (2023), Investigation of ^{22}Mg levels via resonant scattering of ^{18}Ne + α.
Front. Phys. 11:1163299.
doi: 10.3389/fphy.2023.1163299

Investigation of ^{22}Mg levels via resonant scattering of ^{18}Ne + α

S. M. Cha[1,2], K. Y. Chae[1]*, K. Abe[3], S. Bae[2,4], D. N. Binh[5], S. H. Choi[4], N. N. Duy[1,6], Z. Ge[7,8], K. I. Hahn[2,9], S. Hayakawa[3], B. Hong[10], N. Iwasa[7,11], D. Kahl[12,13], L. H. Khiem[14,15], A. Kim[10,16], D. Kim[2,16], E. J. Kim[17], G. W. Kim[16,18], M. J. Kim[1], K. Kwak[19], M. S. Kwag[1,20], E. J. Lee[1], S. I. Lim[16], B. Moon[2,10], J. Y. Moon[20], S. Y. Park[16,18], V. H. Phong[7], H. Shimizu[3], H. Yamaguchi[3] and L. Yang[3]

[1]Department of Physics, Sungkyunkwan University, Suwon, Republic of Korea, [2]Center for Exotic Nuclear Studies, Institute for Basic Science, Daejeon, Republic of Korea, [3]Center for Nuclear Study, The University of Tokyo, Wako, Japan, [4]Department of Physics and Astronomy, Seoul National University, Seoul, Republic of Korea, [5]30 MeV Cyclotron Center, Tran Hung Dao Hospital, Hanoi, Vietnam, [6]Institute of Postgraduate Program, Van Lang University, Ho Chi Minh, Vietnam, [7]RIKEN Nishina Center, Wako, Japan, [8]GSI Helmholtzzentrum für Schwerionenforschung GmbH, Darmstadt, Germany, [9]Department of Science Education, Ewha Womans University, Seoul, Republic of Korea, [10]Department of Physics, Korea University, Seoul, Republic of Korea, [11]Department of Physics, Tohoku University, Sendai, Japan, [12]School of Physics and Astronomy, University of Edinburgh, Edinburgh, United Kingdom, [13]Extreme Light Infrastructure-Nuclear Physics, Horia Hulubei National Institute for R&D in Physics and Nuclear Engineering (IFIN-HH), Bucharest-Magurele, Romania, [14]Institute of Physics, Vietnam Academy of Science and Technology, Hanoi, Vienam, [15]Graduate University of Science and Technology, Vietnam Academy of Science and Technology, Hanoi, Vienam, [16]Department of Physics, Ewha Womans University, Seoul, Republic of Korea, [17]Division of Science Education, Jeonbuk National University, Jeonju, Republic of Korea, [18]Center for Underground Physics, Institute for Basic Science, Daejeon, Republic of Korea, [19]Department of Physics, College of Natural Sciences, Ulsan National Institute of Science and Technology (UNIST), Ulsan, Republic of Korea, [20]Rare Isotope Science Project, Institute for Basic Science, Daejeon, Republic of Korea

The α resonant scattering on ^{18}Ne was measured in inverse kinematics to understand the α-clustering of proton-rich ^{22}Mg nucleus, performed at the CNS Radio-Isotope Beam Separator (CRIB) of Center for Nuclear Study, University of Tokyo, located at the RIBF of RIKEN Nishina Center. The excitation function of ^{22}Mg was obtained for the excitation energies of 10–16 MeV by adopting the thick-target method. Several resonances were evident in the present work, which implies the existence of energy levels with large α widths. Since energy levels were not clearly observed at the astrophysically important energy range, upper limits on the ^{18}Ne $(\alpha, \alpha)^{18}$Ne cross section were set. The astrophysical impact was also investigated by estimating the ^{18}Ne $(\alpha, p)^{21}$Na cross section.

KEYWORDS

nuclear cluster, α-cluster structure, resonant scattering, energy level properties, thick-target method in inverse kinematics, RI beam, explosive stellar environments, ^{18}Ne(a,p)^{21}Na

1 Introduction

The α-cluster structure in atomic nuclei has been one of the most interesting topics in nuclear physics. The α-clusterization of self-conjugate ($N = Z$) and $A = 4n$ ($n = 2, 3, 4, \cdots$) nuclei including ^{8}Be, ^{12}C, ^{16}O, and ^{20}Ne has been studied extensively for decades [1–3]. The strong evidence for the α-cluster structure was found through the studies. Observations of a series of levels with large α reduced widths that form a rotational band can provide a convincing probe for α-cluster configuration in the nuclei. The development of theoretical models and rare isotope beams has provided significant opportunities to extend our knowledge of the α-cluster structure in exotic nuclei. Experimental investigations on the α-clusterization of neutron-rich nuclei, including ^{10}Be, ^{12}Be, and ^{14}C, have been performed [4–6]. These studies have substantially improved our understanding of the α-cluster structure in neutron-rich nuclei; however, α-cluster studies of proton-rich (neutron-deficient) nuclei have not been sufficiently established. Considering the isobaric invariance of the nuclear force, the characteristics of the α-cluster structure for a proton-rich nucleus are similar to those for its mirror nucleus. For example, experimental results indicate that some of the observed resonances in ^{11}C may originate from the negative-parity cluster band, which is analogous to its mirror nucleus ^{11}B [7, 8].

The α-cluster structure of neutron-rich ^{22}Ne has been extensively investigated both experimentally and theoretically [9–13]. Rogachev *et al.* observed a splitting of 1^-, 3^-, 7^-, and 9^- α-cluster states into doublets [10], which could be theoretically explained by the extended two cluster model (ETCM) calculation assuming the α + ^{18}O two-cluster configuration [11]. Recently, Kimura suggested the presence of two kinds of α-cluster structures in ^{22}Ne using the hybrid-generator coordinate method (GCM) calculation. The first is the molecular orbital bands with the α + ^{16}O core and two valence neutrons, which correspond to the observed α-cluster states below the α + ^{18}O threshold energy reported in [14, 15]. The other is the α + ^{18}O molecular bands, which correspond to the observed states above the threshold energy reported in Ref. [10].

Studies on the α-cluster structure of proton-rich ^{22}Mg are still very rare. The GCM calculation predicted the existence of the 1^- and 3^- doublet states located at excitation energies of 12–13 MeV, assuming the α + ^{18}Ne two-cluster model [11]. Considering the lower energy level density of proton-rich nuclei than that of neutron-rich nuclei, observing doublets should be easier in the case of the ^{22}Mg nucleus. However, the experimental data obtained by Goldberg *et al.* [12] show no clear evidence of the doublets. Although the excitation function of mirror nucleus ^{22}Ne in [12] show the existence of the strong 1^- and 3^- doublets originating from the α-clustering, the excitation function of ^{22}Mg is rather featureless. The authors could not specify the reason for the absence of the doublets since the quality of the ^{22}Mg data was not sufficient for independent analysis.

A powerful approach for investigating the α-cluster structure in the ^{22}Mg nucleus is to populate α-cluster states by resonant elastic scattering of ^{18}Ne and α. Therefore, we measured ^{18}Ne + α resonant scattering using ^{18}Ne rare isotope beam to identify predicted 1^- and 3^- doublets. The excited states of ^{22}Mg have been extensively investigated by various nuclear reactions, including ^{12}C (^{16}O, ^{6}He) ^{22}Mg [16]; ^{24}Mg (p, t)^{22}Mg [17, 18]; ^{18}Ne (α, p)^{21}Na [19–21]; and ^{21}Na (p, p)^{21}Na [22–24]. The α partial widths are, however, not known for most levels, which cannot provide a clear evidence of the α-clusterization in the ^{22}Mg nucleus. In the present study, the excitation function of ^{22}Mg was obtained for excitation energies of E_x ~ 10–16 MeV, which can provide important information about the energy level properties including α partial widths.

Investigating the spectroscopic information of ^{22}Mg also plays a crucial role in understanding the astrophysically important ^{18}Ne (α, p)^{21} Na reaction because the reaction occurs through the resonances in the compound nucleus. The ^{18}Ne (α, p)^{21}Na reaction is known as one of the possible breakout routes from the hot-CNO cycles, which leads the rapid proton capture (rp) process [25–27]. In a recent sensitivity study by Cyburt *et al.*, the ^{18}Ne (α, p)^{21}Na reaction was identified as one of the most important reactions which impact on the X-ray burst light curve and the composition of burst ashes [28]. Considering the typical X-ray burst temperature of T ~ 2 GK, the Gamow window corresponds to the excitation energy E_x ~ 9.56–10.96 MeV. Therefore, it is important to study the energy level properties of ^{22}Mg in this energy region. The ^{18}Ne (α, p)^{21}Na reaction has been studied by direct measurements [19–21] and time-reversal reaction measurement [29]. The experimental results, however, show a large discrepancy. In the present work, the ^{18}Ne (α, p)^{21}Na reaction cross section was estimated based on the experimental level structure of the ^{22}Mg nucleus.

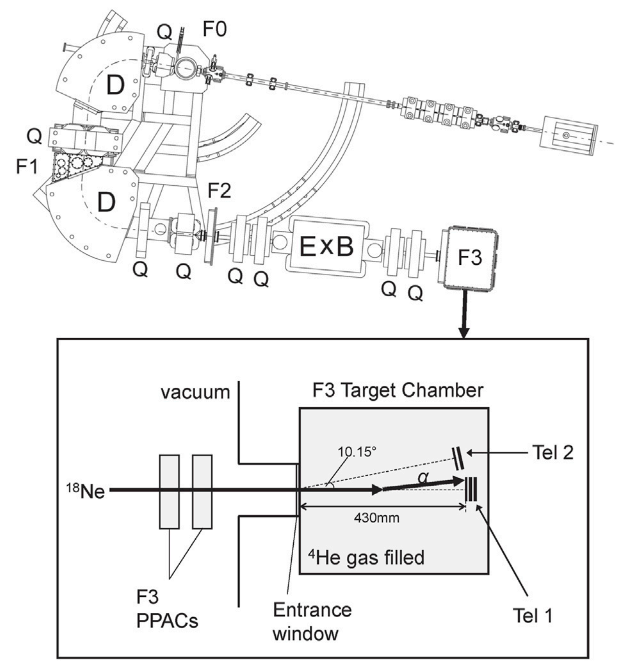

FIGURE 1
Schematic view of the CRIB separator (top) and the experimental setup for the ^{18}Ne + α resonant scattering measurement at the F3 focal plane (bottom). The ^{18}Ne beam particles were identified and monitored by two F3 PPACs. ^{4}He gas at 470 Torr was filled to the chamber, which was sealed with a 23-μm-thick Mylar foil as a beam entrance window. The energy and position of the recoiling α particle were measured by ΔE-E silicon detector telescopes (Tel 1 and Tel 2).

2 Experiment

The α resonant elastic scattering of ^{18}Ne was measured in inverse kinematics at the CNS Radio-Isotope Beam Separator (CRIB) [30, 31] of the Center for Nuclear Study, University of Tokyo, located at the RIBF of RIKEN Nishina Center. A schematic of the experimental setup is shown in Figure 1. The ^{18}Ne rare isotope beam was produced by using the in-flight (IF) method. A primary ^{16}O beam with an energy of 8.026 MeV/u from the AVF cyclotron [32] was delivered to the F0 focal plane of CRIB and bombarded a ^{3}He gas target. Then, a secondary ^{18}Ne beam was produced by the ^{3}He (^{16}O, ^{18}Ne)n reaction. The ^{3}He gas was contained in the cell at a pressure of 360 Torr. The ^{3}He gas atoms were isolated from the beam line kept at a high-level vacuum by using 2.5-μm-thick Havar foils as the entrance and exit windows. To increase the density of the ^{3}He gas target and the intensity of the secondary ^{18}Ne beam, a cryogenic system using liquid nitrogen was used [33]. The areal thickness of the ^{3}He gas target was achieved to be 1.54 mg/cm^2 by keeping the temperature at T ~90 K.

^{18}Ne^{10+} ions were selected by a double achromatic system with a proper magnetic rigidity ($B\rho$) value of 0.5920 Tm, which is optimized to obtain the maximum ^{18}Ne beam production rate. A slit of ±15 mm was installed at the momentum dispersive focal plane (F1) to remove the beam contaminations produced due to various nuclear reactions, yielding the momentum dispersion $\Delta p/p$ ~ 1%. The secondary beam particles were further purified using the Wien Filter (WF) system by applying a high voltage of ±59.5 kV. Two delay-line-type PPACs [34] were installed downstream of the WF to measure the time and the two-dimensional position information for each secondary beam particle. By using PPACs, the secondary beam identification after the WF was performed. The ^{18}Ne beam intensity and purity were ~2.6 × 10^5 pps and ~ 65%, respectively. The impurities were ^{17}F^{9+} (~ 28%) and ^{16}O^{8+} (~ 4%), respectively. A small amount of other beam species including ^{15}O^{8+}, ^{13}N^{7+}, and ^{4}He^{2+} was also observed. These contaminants were clearly excluded by the time-of-flight information in the final analysis.

The F3 target chamber was filled with ^{4}He gas for α scattering measurement. The ^{4}He gas was at a pressure of 470 Torr and was sealed with a 23-μm-thick aluminized Mylar foil as a beam entrance window. The ^{4}He target pressure was selected to stop the ^{18}Ne beam before it reaches the detector. The ^{18}Ne beam energy after passing through the target entrance window was measured as 45.2 ± 1.1 MeV, which is consistent with an energy loss calculation result considering the $B\rho$ value of 0.5920 Tm and the effective thickness of ~ 45 μm Mylar foil for the two PPACs and the beam entrance window. By adopting the thick-target method in inverse kinematics [35], a wide range of excitation energies of ^{22}Mg was investigated with a single ^{18}Ne beam energy.

The energy and position of the recoiling α particles were obtained using two sets of ΔE-E silicon detector telescopes. The central telescope (Tel 1) was installed at 430 mm downstream from the entrance window of the target chamber along the beam axis. The other telescope (Tel 2) was located at 10.15° off from the beam axis, as viewed from the center of the entrance window. Tel 1 (Tel 2) consisted of 20-μm-, 496-μm-, and 485-μm-thick (20-μm- and 1500-μm-thick) silicon detectors. The most energetic α particles from the ^{18}Ne (α, α)^{18}Ne reaction could be entirely stopped under these conditions. Each detector had 16 strips and an active area of 50 × 50 mm^2. Energy calibration of each strip was carried out by using an α-emitting source composed of ^{148}Gd (3.148 MeV), ^{241}Am (5.462 MeV), and ^{244}Cm (5.771 MeV). Since the energy range of recoiling α particles is much wider (0–27 MeV) than that of the α particles from the source, additional energy calibration was required for the high-energy region. α beams at various energies (13, 15, 20, and 25 MeV) were used for this purpose.

Even after the beam purification using the CRIB spectrometer, beam-like α particles were transported to the F3 reaction target chamber. These beam-like α particles were produced at the upstream of the beam line and selected by the $B\rho$ value which was set for the ^{18}Ne beam particles of interest. The number of the beam-like α particles was much less than the number of ^{18}Ne beam particles (≪ 0.01%); however, an amount comparable to that of the reaction products reached the central telescope. Therefore, the argon target was used for the background measurement. The argon gas pressure of about 87 Torr was selected so that the incident particles exhibit energy losses similar to those of ^{4}He gas. By comparing the two α spectra obtained with and without the ^{4}He gas target, the contribution from beam-like α particles was identified.

3 Data analysis

3.1 Kinematics reconstruction

The particle identification was performed by the standard energy loss techniques. A typical particle identification plot obtained at the central telescope is shown in Figure 2. The total energy deposition of the particles is plotted as a function of energy deposition in the ΔE detector. As shown in the figure, α particles were clearly separated without significant contamination from other charged particle groups. The α particles with E_{tot} ~ 13 MeV were observed in the background run with argon gas, as shown in Figure 2B, indicating that those α particles were contaminants in the secondary beams. The beam-like α particles were clearly distinguished by using the time-of-flight information between the PPAC and the second layer of the telescope, as shown in Figure 3.

The α particles in coincidence with the ^{18}Ne beams incident in the target chamber were selected for further analysis. The measured energy of the α particle (E_α) was converted to the center-of-mass energy of ^{18}Ne + α system ($E_{\mathrm{c.m.}}$) by assuming the elastic scattering kinematics using

$$E_{\mathrm{c.m.}} = \frac{M_{\mathrm{Ne}} + M_\alpha}{4M_{\mathrm{Ne}}\cos^2\theta_{\mathrm{lab}}} E_\alpha, \tag{1}$$

where M_{Ne} and M_α are the nuclear masses of the ^{18}Ne and α particle, respectively, and θ_{lab} is the scattering angle in the laboratory frame. The value of θ_{lab} was determined using the trajectories of the recoiling α particle and corresponding ^{18}Ne beam particle at the reaction vertex. The reaction vertex in the extended gas target was reconstructed by considering the energy losses of the ^{18}Ne beam and recoiling α particle in ^{4}He gas. The energy loss functions were obtained using the SRIM code [36]. Direct measurement of the energy loss of the ^{18}Ne beam at six different target pressures in the present study was in good agreement with the SRIM calculation result.

3.2 Excitation function of ^{18}Ne + α elastic scattering

The differential cross section of ^{18}Ne + α resonant elastic scattering in the center-of-mass frame was calculated by

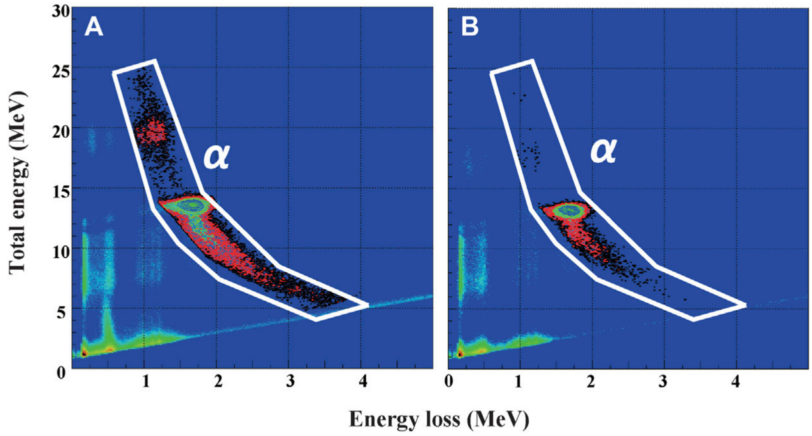

FIGURE 2
A typical particle identification plot is shown. The total energy of a recoiling particle is plotted as a function of the energy deposition in the first layer of the telescope. Events in the region with thick solid lines are identified as α particles from **(A)** ^{4}He and **(B)** argon gas run.

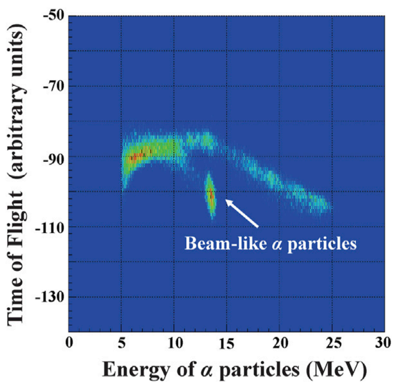

FIGURE 3
The ToF between the F3 PPAC and the second layer of the Tel 1 is plotted as a function of the energy of α particles. The beam-like α particles from the upstream were clearly separated from the recoiling α particles. The slope-like dependence observed at high energies is due to the slewing effect (which is not corrected in this plot).

$$\left(\frac{d\sigma}{d\Omega}\right)_{\mathrm{c.m.}} = \frac{1}{4\cos\theta_{\mathrm{lab}}}\left(\frac{d\sigma}{d\Omega}\right)_{\mathrm{lab}} = \frac{1}{4\cos\theta_{\mathrm{lab}}}\frac{Y}{IN\Delta\Omega_{\mathrm{lab}}}, \quad (2)$$

where Y is the yield of recoiling α particles, θ_{lab} is the scattering angle in the laboratory frame, I is the number of ^{18}Ne beam particles incident on the target, N is the number of ^{4}He target atoms, and $\Delta\Omega_{\mathrm{lab}}$ is the solid angle covered by the detector.

The number of incident ^{18}Ne beam particles was counted using two F3 PPACs. To obtain the precise number of beam particles entering into the target chamber through the entrance window, an additional cut was applied to the ^{18}Ne beam events. The positions of the beam particles at the target entrance were reconstructed event-by-event by extrapolating the beam trajectory obtained at two F3 PPACs, and then ^{18}Ne beam events falling in the diameter of the entrance of the target chamber were selected. A total of ~ 1.33×10^{10} ^{18}Ne beam ions impinged on the target during the runs.

The excitation function of ^{18}Ne + α resonant elastic scattering was extracted by selecting α events with an angular range of $0^\circ \leq \theta_{\mathrm{lab}} \leq 7^\circ$ ($166^\circ \leq \theta_{\mathrm{c.m.}} \leq 180^\circ$). The solid angle was calculated using the known detector geometry and reaction vertex of each event as a function of $E_{\mathrm{c.\,m.}}$. Due to the finite angular range of θ_{lab}, an average value of solid angle at the reaction vertex (or $E_{\mathrm{c.\,m.}}$) was used. The areal number density of ^{4}He atoms was obtained by considering the effective target thickness as a function of $E_{\mathrm{c.\,m.}}$. The uncertainty in $E_{\mathrm{c.\,m.}}$ was measured to be approximately 50–100 keV, depending on the energy. The uncertainty originates from the energy resolution of a silicon detector (30–90 keV) and energy straggling of the ^{18}Ne beam and α particles in the gas (20–60 keV).

3.3 Upper limits on the cross section

The ^{18}Ne $(\alpha, \alpha)^{18}$Ne cross section extracted in the present work is rather smooth in the energy region below $E_{\mathrm{c.\,m.}} < 3$ MeV. In this region, however, two small bumps were observed at $E_{\mathrm{c.\,m.}}$ ~2.6 MeV and 2.7 MeV in the cross section spectrum. Several resonances in ^{22}Mg have been identified in the energy range through the previous ^{18}Ne $(\alpha, p)^{21}$Na reaction study as reported in [20]. For instance, two energy levels located at the resonance energies of E_r = 2.52 ± 0.14 MeV and E_r = 2.72 ± 0.14 MeV have been reported in the previous direct measurement by Groombridge et al. [20]. However, the existence of these resonances is not obvious in our data, possibly due to the insufficient statistics. Therefore, the upper limits on the cross section were set to indicate the possible maximum resonant cross section that is consistent with our experimental spectrum. Figure 4 shows the obtained upper limits by assuming hypothetical levels located at $E_{\mathrm{c.\,m.}}$ = 2.63 MeV (top) and $E_{\mathrm{c.\,m.}}$ = 2.75 MeV (middle). The upper limit with both hypothetical levels is also plotted in the figure (bottom). The black circles represent the empirical cross sections obtained at $0^\circ \leq \theta_{\mathrm{lab}} \leq 7^\circ$. The blue solid lines represent the best fit curves for the observed bumps. The

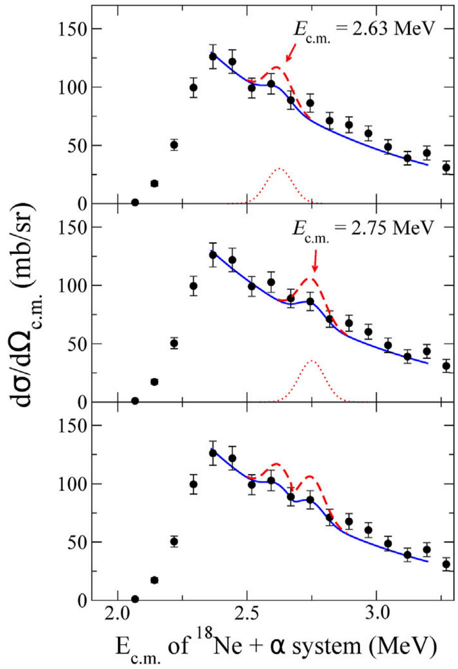

FIGURE 4
The upper limits of the ^{18}Ne (α, α)^{18}Ne cross section by assuming hypothetical levels located at $E_{c.\,m.}$ = 2.63 MeV (top) and $E_{c.\,m.}$ = 2.75 MeV (middle) are plotted as red dashed lines. The upper limit with both resonances is also plotted (bottom). The one-sigma confidence level was considered to obtain the upper limit. The black circles represent the experimental excitation function obtained at 0° ≤ θ_{lab} ≤ 7°, the blue solid line represents the best fitting result of it, and the red dotted line represents each hypothetical level.

TABLE 1 The resonance parameters used in the ^{18}Ne (α, p)^{21}Na cross section calculation are summarized. Two sets of parameters ("COM1" and "COM2") are used in the calculation to illustrate the sensitivity of the Γ_p for the reaction cross section. All energies are expressed in MeV.

	E_r	J^π	Γ_α	Γ_p	Γ_{tot}
COM1	2.63	0⁺	0.015	0.01	0.025
	2.75	0⁺	0.015	0.01	0.025
COM2	2.63	0⁺	0.015	0.085	0.1
	2.75	0⁺	0.015	0.195	0.21

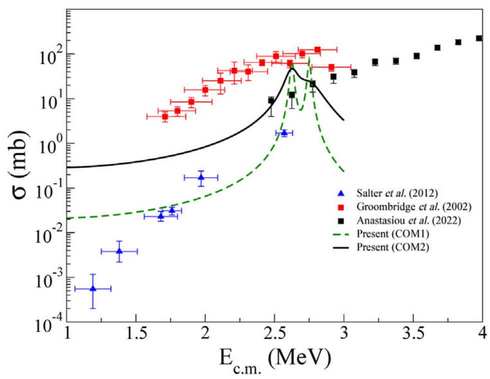

FIGURE 5
Comparison of the ^{18}Ne (α, p)^{21}Na reaction cross section calculations in the present work with the previous measurements by Salter et al. [29], Groombridge et al. [20], and Anastasiou et al. [21] is shown.

reduced χ^2 value of the best fit curve is 0.893. The shape of the resonance was assumed to be Gaussian, as plotted as a red dotted line in the figure, because the broadening by the experimental resolution is expected to dominate the width. The width of the Gaussian was assumed to be 50 keV to fit the observed bumps. The normalization factor of the distribution was then increased until the χ^2 value decreased to a prescribed amount, resulting in a one-sigma confidence level. The red dashed lines represent the upper limits of the ^{18}Ne (α, α)^{18}Ne cross section. A fluctuation of experimental data points was also observed at $E_{c.\,m.}$ ~ 2.9 MeV. This bump could be a corresponding resonance at E_r = 2.87 ± 0.14 MeV reported in a previous work [20]; however, it does not fall into the Gamow window at T ~ 2 GK. Therefore, the upper limit was not evaluated for this resonance.

4 Discussion

4.1 Astrophysical implication

Two small bumps observed in the present work fall within the Gamow window of the astrophysically important ^{18}Ne (α, p)^{21}Na reaction relevant to a temperature of T ~ 2 GK. The contribution of the observed bumps to the ^{18}Ne (α, p)^{21}Na reaction was then investigated. The cross section of the ^{18}Ne (α, p)^{21}Na reaction was calculated using the Breit–Wigner formula [37].

$$\sigma_{BW}(E) = \frac{\lambda^2}{4\pi}\frac{(2J_r+1)}{(2J_{\mathrm{Ne}}+1)(2J_\alpha+1)}\frac{\Gamma_\alpha\Gamma_p}{(E-E_r)^2+(\Gamma_{\mathrm{tot}}/2)^2}, \qquad (3)$$

where λ is the de Broglie wavelength; E_r is the resonance energy; J, J_{Ne}, and J_α are the spins of resonance, ^{18}Ne, and ^{4}He, respectively. Γ_α, Γ_p, and Γ_{tot} are the α partial width, proton partial width, and total width, respectively. $\Gamma_{\mathrm{tot}} = \Gamma_\alpha + \Gamma_p$ was assumed in the calculations. Two hypothetical levels used in the upper limit calculation were considered to be the resonances for the ^{18}Ne (α, p)^{21}Na reaction, where the resonance energies were adopted as E_r = 2.63 and 2.75 MeV. Γ_α values of both resonances were determined by further analyzing with the R-matrix code SAMMY8 [38, 39], where the experimental energy increase of ~ 50 keV was assumed. The best fit yielded values of Γ_α = 15 keV for both resonances. The spin and parity of both resonances was adopted as $J^\pi = 0^+$ while calculating the cross section. Several J^π values for the resonances located in the astrophysically important energy region have been suggested in the previous direct measurement by Groombridge et al. [20], including $J^\pi = 0^+$. However, the choice of other J^π values such as $J^\pi = 1^-$ or 2^+ for observed bumps would imply our Γ_α which exceed the Wigner limit. Table 1 summarizes the resonance parameters used in the ^{18}Ne (α, p)^{21}Na cross section calculations.

Although proton resonant scattering on the ^{21}Na nucleus has been measured in literatures [22–24], Γ_p in the corresponding energy

10.3389/fphy.2023.1163299

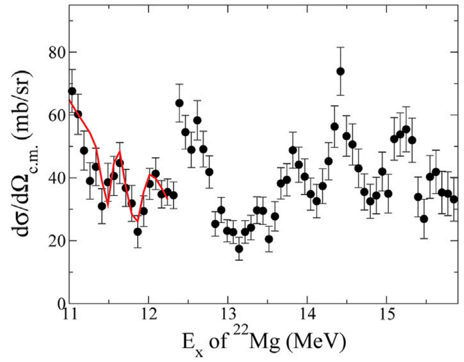

FIGURE 6
The excitation function of the elastic scattering of α particles on ^{18}Ne obtained at 0°≤ θ_{lab} ≤7° (black circles) with the R-matrix fit with three resonances (red solid line) is shown.

region has not been reported so far. To approximate Γ_p values for the resonances, the Wigner limit for the proton was calculated by $\Gamma_w = 2\hbar^2/\mu R^2 P_l$, where μ is the reduced mass, R is the interaction radius, and P_l is the penetrability of a given orbital angular momentum l. An interaction radius of $R = 1.35\ (1 + 21^{1/3})$ fm [24] was adopted in the calculation. By considering the global mean reduced proton width $\theta_p^2 = 0.0045$, suggested in [40], Γ_p was estimated to be ~10 keV for the resonances at E_r = 2.63 and 2.75 MeV, which is summarized as "COM1" in Table 1. To illustrate the sensitivity of the proton widths for the ^{18}Ne $(\alpha, p)^{21}$Na reaction cross section, another set of Γ_p values for the resonances was approximated by assuming $\Gamma_p = \Gamma_{tot} - \Gamma_\alpha$ ("COM2" in Table 1). We adopted Γ_{tot} = 0.1 MeV (Γ_{tot} = 0.21 MeV) for the resonance at E_r = 2.63 MeV (E_r = 2.75 MeV), as reported in the previous direct measurement by Groombridge *et al.* [20].

The calculation results for the ^{18}Ne $(\alpha, p)^{21}$Na reaction cross section are shown in Figure 5, in comparison with the previous experimental results. The cross sections deduced by the Breit–Wigner formula using two sets of Γ_p values are shown as the green dashed and black solid lines, respectively. The blue triangles represent the experimental data obtained by Salter et al. [29], which were determined from the time-reversal reaction measurement. The ^{18}Ne $(\alpha, p_0)^{21}$Na reaction cross section was inferred by using the principle of the detailed balance theorem [41]; therefore, their data can provide a lower limit for the cross section. The red squares represent the ^{18}Ne $(\alpha, p)^{21}$Na cross section derived from the resonance parameters reported by Groombridge et al. [20]. The black squares represent the recent direct measurement results by Anastasiou et al. [21], which shows a lower cross section by almost an order of magnitude compared with that of Groombridge et al. As shown in the figure, our calculation results indicate that the ^{18}Ne $(\alpha, p)^{21}$Na reaction cross section depends critically on the proton widths of the resonances in the astrophysically important energy region. Thus, experimental studies of the Γ_p are highly required for a conclusive understanding of the ^{18}Ne $(\alpha, p)^{21}$Na reaction cross section.

4.2 *R*-matrix analysis and α-cluster structure

The excitation function of ^{18}Ne + α elastic scattering obtained at the higher excitation energy region E_x ~ 11–16 MeV is shown in Figure 6. The black circles represent the differential cross sections of the ^{18}Ne $(\alpha, \alpha)^{18}$Ne obtained at $0° \le \theta_{lab} \le 7°$. Several peaks were evident in the spectrum, which implies the existence of resonances with large Γ_α. Since the strength of the α-clustering feature of a resonance state is reflected by its α width, observed peaks in the present work are possible candidates of α-cluster states. To constrain the energy level properties of ^{22}Mg including Γ_α, an analysis using the *R*-matrix calculation code SAMMY8 [38, 39] has been in progress. A channel radius of R_c = 5.0 fm was adopted in the calculation, which is the same value used in the GCM calculation [11]. We calculated the excitation function at an average angle of $\theta_{c.m.}$ = 173 °, and the result was then broadened considering the experimental energy resolution.

By introducing three resonances in the *R*-matrix calculation, the fitting curve was obtained at $E_x \le 12.3$ MeV, which is plotted as red solid line in Figure 6. The resonance parameters are summarized in Table 2. Since the spectroscopic information of ^{22}Mg nucleus in this energy region is very limited, an intensive *R*-matrix analysis with all possible spin and natural parity combinations for observed resonances should be carefully performed until the experimental excitation function is well-reproduced. The resonance parameters with best fitting result will be provided in the future. The χ^2 analysis will be performed to deduce possible parameters for each peak. The dimensionless partial width θ_a^2 for each level will be calculated by $\theta_a^2 = \Gamma_\alpha/\Gamma_W$, where Γ_W is the Wigner limit of Γ_α, which can provide a direct comparison with theoretical predictions in [11]. More detailed calculations would be necessary to reveal the nature of those levels, if they are shell-model-like or cluster-like states.

TABLE 2 Resonance properties of ^{22}Mg extracted from the present work are summarized. Results from the previous works are listed for comparison.

Present work			Goldberg et al. [12]		Dufour and Descouvemont [11]		
E_x	Γ_α	J^π	E_x	J	E_x^{GCM}	J^π	θ^2_{GCM}
(MeV)	(keV)		(MeV)		(MeV)		(%)
11.49	7	1^-	11.462	1	12.25	1^-	11.5
11.71	3	3^-	11.798	2	12.57	3^-	11.6
11.87	6	1^-	11.842	1	13.15	1^-	6.7
					13.30	3^-	11.7

5 Summary

We measured α resonant elastic scattering on ^{18}Ne using the thick-target method in inverse kinematics technique to improve our knowledge of the α-cluster structure of proton-rich ^{22}Mg nucleus. The excitation function for ^{18}Ne $(\alpha, \alpha)^{18}$Ne in the energy range of E_x ~ 10–16 MeV was obtained at $0^\circ \le \theta_{lab} \le 7^\circ$. Several levels with large α widths were evident in our result, which can be candidates for the α-cluster states. To clarify the energy level properties of ^{22}Mg and to investigate α-clustering features, the R-matrix analysis is in progress. The resonance parameters will be extracted considering all possible combinations of spin and parity for observed peaks. The first experimental constraints on spectroscopic information of ^{22}Mg above E_x ~ 13 MeV will be provided. To better understand the experimental results, complete theoretical descriptions are required in the future.

No levels were evident at E_x < 11 MeV in the present work, even though two small bumps were observed in the cross section spectrum. Therefore, we set upper limits on the ^{18}Ne $(\alpha, \alpha)^{18}$Ne cross section, which indicate the possible maximum resonant cross section assuming the hypothetical levels at E_x = 10.772 and 10.892 MeV ($E_{c.m.}$ = 2.63 and 2.75 MeV). We also estimated the astrophysically important ^{18}Ne $(\alpha, p)^{21}$Na reaction cross section based on our experimental data. The calculation indicates that the ^{18}Ne $(\alpha, p)^{21}$Na cross section depends on the proton widths of the resonances as well. Experimental studies on Γ_p are necessary to evaluate the ^{18}Ne $(\alpha, p)^{21}$Na reaction cross section conclusively.

Data availability statement

The raw data supporting the conclusion of this article will be made available by the authors, without undue reservation.

Author contributions

KC was the spokesperson of the experiment. All authors contributed to the setup of the experiment and the measurements. SMC wrote the first draft, the revised versions, and the final version of the manuscript. All authors listed have made a substantial, direct, and intellectual contribution to the work and approved it for publication.

Funding

This work was supported by the Institute for Basic Science (IBS) funded by the Ministry of Science and ICT, Korea (Grant No. IBS-R031-D1). This work was also supported by the National Research Foundation of Korea (NRF) grant funded by the Korean Government (MSIT) Nos. 2020R1A2C1005981 and 2019K2A9A2A10018827. This work has been supported by the Rare Isotope Science Project of Institute for Basic Science funded by the Ministry of Science and NRF of Korea (2013M7A1A1075765). AK acknowledges the National Research Foundation of Korea (NRF) grants funded by the Korean Government (Grant No. 2018R1A5A1025563). LHK acknowledges the support of the International Centre of Physics at the Institute of Physics (Grant No. ICP.2023.04).

Acknowledgments

The experiment was performed at the RIBF operated by RIKEN Nishina Center and CNS, University of Tokyo. The authors are grateful to the RIKEN and CNS accelerator staff for their technical support.

Conflict of interest

The authors declare that the research was conducted in the absence of any commercial or financial relationships that could be construed as a potential conflict of interest.

Publisher's note

References

1. Ikeda K, Takigawa N, Horiuchi H. The systematic structure-change into the molecule-like structures in the self-conjugate \$4n\$ nuclei. *Prog Theor Phys Suppl* (1968) E68:464–75. doi:10.1143/PTPS.E68.464

2. Freer M. The clustered nucleus—Cluster structures in stable and unstable nuclei. *Rep Prog Phys* (2007) 70:2149–210. doi:10.1088/0034-4885/70/12/R03

3. Horiuchi H, Ikeda K, Katō K. Recent developments in nuclear cluster physics. *Prog Theor Phys Suppl* (2012) 192:1–238. doi:10.1143/PTPS.192.1

4. Freer M, Angélique JC, Axelsson L, Benoit B, Bergmann U, Catford WN, et al. Exotic molecular states in ^{12}Be. *Phys Rev Lett* (1999) 82:1383–6. doi:10.1103/PhysRevLett.82.1383

5. Freer M, Angélique JC, Axelsson L, Benoit B, Bergmann U, Catford WN, et al. Helium breakup states in ^{10}Be and ^{12}Be. *Phys Rev C* (2001) 63:034301. doi:10.1103/PhysRevC.63.034301

6. Yamaguchi H, Kahl D, Hayakawa S, Sakaguchi Y, Abe K, Nakao T, et al. Experimental investigation of a linear-chain structure in the nucleus ^{14}C. *Phys Lett B* (2017) 766:11–6. doi:10.1016/j.physletb.2016.12.050

7. Yamaguchi H, Hashimoto T, Hayakawa S, Binh DN, Kahl D, Kubono S, et al. α resonance structure in ^{11}B studied via resonant scattering of ^{7}Li+α. *Phys Rev C* (2011) 83: 034306. doi:10.1103/PhysRevC.83.034306

8. Yamaguchi H, Kahl D, Wakabayashi Y, Kubono S, Hashimoto T, Hayakawa S, et al. α-resonance structure in ^{11}C studied via resonant scattering of ^{7}Be + α and with the ^{7}Be(α, p) reaction. *Phys Rev C* (2013) 87:034303. doi:10.1103/PhysRevC.87.034303

9. Descouvemont P. Microscopic investigation of the α+^{18}O system in a three-cluster model. *Phys Rev C* (1988) 38:2397–407. doi:10.1103/PhysRevC.38.2397

10. Rogachev GV, Goldberg VZ, Lönnroth T, Trzaska WH, Fayans SA, Källman KM, et al. Doubling of α-cluster states ^{22}Ne. *Phys Rev C* (2001) 64:051302. doi:10.1103/PhysRevC.64.051302

11. Dufour M, Descouvemont P. Microscopic study of α-cluster states in ^{22}Ne. *Nucl Phys A* (2003) 726:53–66. doi:10.1016/j.nuclphysa.2003.07.004

12. Goldberg VZ, Rogachev GV, Trzaska WH, Kolata JJ, Andreyev A, Angulo C, et al. Investigation of the α-cluster structure of ^{22}Ne and ^{22}Mg. *Phys Rev C* (2004) 69:024602. doi:10.1103/PhysRevC.69.024602

13. Kimura M. Molecular orbitals and α +^{18}O molecular bands of ^{22}Ne. *Phys Rev C* (2007) 75:034312. doi:10.1103/PhysRevC.75.034312

14. Scholz W, Neogy P, Bethge K, Middleton R. 0^+ state at 6.24 MeV in ^{22}Ne excited by the reaction ^{18}O(^{7}Li,*t*)^{22}Ne. *Phys Rev Lett* (1969) 22:949–51. doi:10.1103/PhysRevLett.22.949

15. Scholz W, Neogy P, Bethge K, Middleton R. Rotational bands in ^{22}Ne excited by the ^{18}O(^{7}Li,*t*)^{22}Ne reaction. *Phys Rev C* (1972) 6:893–900. doi:10.1103/PhysRevC.6.893

16. Chen AA, Lewis R, Swartz KB, Visser DW, Parker PD. Structure of ^{22}Mg and its implications for explosive nucleosynthesis. *Phys Rev C* (2001) 63:065807. doi:10.1103/PhysRevC.63.065807

17. Chae KY, Bardayan DW, Blackmon JC, Chipps KA, Hatarik R, Jones KL, et al. Constraint on the astrophysical ^{18}Ne(α,p)^{21}Na reaction rate through a ^{24}Mg(p,t)^{22}Mg measurement. *Phys Rev C* (2009) 79:055804. doi:10.1103/PhysRevC.79.055804

18. Matic A, Berg AM, Harakeh MN, Wörtche HJ, Berg GPA, Couder M, et al. High-precision (p, t) reaction measurement to determine ^{18} Ne(α,p)^{21}Na reaction rates. *Phys Rev C* (2009) 80:055804. doi:10.1103/PhysRevC.80.055804

19. Bradfield-Smith W, Davinson T, DiPietro A, Laird AM, Ostrowski AN, Shotter AC, et al. Breakout from the hot CNO cycle via the ^{18} Ne(α,p)^{21}Na reaction. *Phys Rev C* (1999) 59:3402–9. doi:10.1103/PhysRevC.59.3402

20. Groombridge D, Shotter AC, Bradfield-Smith W, Cherubini S, Davinson T, Di Pietro A, et al. Breakout from the hot CNO cycle via the ^{18} Ne(α,p)^{21}Na reaction. II. Extended energy range $E_{c.m.}$ ~ 1.7 – 2.9MeV. *Phys Rev C* (2002) 66:055802. doi:10.1103/PhysRevC.66.055802

21. Anastasiou M, Wiedenhöver I, Blackmon JC, Baby LT, Caussyn DD, Hood AA, et al. Measurement of the ^{18} Ne(α,p)^{21}Na reaction with the ANASEN active-target detector system at $E_{c.m.}$ = 2.5 – 4MeV. *Phys Rev C* (2022) 105:055806. doi:10.1103/PhysRevC.105.055806

22. He JJ, Kubono S, Teranishi T, Hu J, Notani M, Baba H, et al. Investigation of excited states in ^{22}Mg via resonant elastic scattering of ^{21}Na + p and its astrophysical implications. *Phys Rev C* (2009) 80:015801. doi:10.1103/PhysRevC.80.015801

23. He JJ, Zhang LY, Parikh A, Xu SW, Yamaguchi H, Kahl D, et al. The ^{18} Ne(α,p) ^{21}Na breakout reaction in x-ray bursts: Experimental determination of spin-parities for α resonances in ^{22}Mg via resonant elastic scattering of ^{21}Na + p. *Phys Rev C* (2013) 88:012801. doi:10.1103/PhysRevC.88.012801

24. Zhang LY, He JJ, Parikh A, Xu SW, Yamaguchi H, Kahl D, et al. Investigation of the thermonuclear ^{18} Ne(α,p)^{21}Na reaction rate via resonant elastic scattering of ^{21}Na + p. *Phys Rev C* (2014) 89:015804. doi:10.1103/PhysRevC.89.015804

25. Wallace RK, Woosley SE. Explosive hydrogen burning. *Astrophys J Suppl Ser* (1981) 45:389–420. doi:10.1086/190717

26. Schatz H, Aprahamian A, Görres J, Wiescher M, Rauscher T, Rembges J, et al. *rp*-process nucleosynthesis at extreme temperature and density conditions. *Phys Rep* (1998) 294:167–263. doi:10.1016/S0370-1573(97)00048-3

27. Woosley SE, Heger A, Cumming A, Hoffman RD, Pruet J, Rauscher T, et al. Models for type I x-ray bursts with improved nuclear physics. *Astrophys J Suppl Ser* (2004) 151:75–102. doi:10.1086/381533

28. Cyburt RH, Amthor AM, Heger A, Johnson E, Keek L, Meisel Z, et al. Dependence of x-ray burst models on nuclear reaction rates. *Astrophys J* (2016) 830:55. doi:10.3847/0004-637X/830/2/55

29. Salter PJC, Aliotta M, Davinson T, Al Falou H, Chen A, Davids B, et al. Measurement of the 18 \mathrm{Ne}({\alpha}{,p_{0}})^{21}\mathrm{Na} reaction cross section in the burning energy region for x-ray bursts. *Phys Rev Lett* (2012) 108:242701. doi:10.1103/PhysRevLett.108.242701

30. Kubono S, Yanagisawa Y, Teranishi T, Kato S, Kishida Y, Michimasa S, et al. New low-energy RIB separator CRIB for nuclear astrophysics. *Eur Phys J A* (2002) 13:217–20. doi:10.1140/epja1339-36

31. Yanagisawa Y, Kubono S, Teranishi T, Ue K, Michimasa S, Notani M, et al. Low-energy radioisotope beam separator CRIB. *Nucl Instrum Methods Phys Res Sect A* (2005) 539:74–83. doi:10.1016/j.nima.2004.09.041

32. Vorozhtsov S, Perepelkin E, Vorozhtsov A, Watanabe S, Kubono S, Goto A. Beam simulations in computer-modelled 3d fields for riken avf cyclotron upgrade. In: Proceedings of Particle Accelerator Society Meeting; August 1-3, 2017; Sapporo, Japan (2009). p. 240–3.

33. Yamaguchi H, Wakabayashi Y, Amadio G, Hayakawa S, Fujikawa H, Kubono S, et al. Development of a cryogenic gas target system for intense radioisotope beam production at CRIB. *Nucl Instrum Methods Phys Res Sect A* (2008) 589:150–6. doi:10.1016/j.nima.2008.02.013

34. Kumagai H, Ozawa A, Fukuda N, Sümmerer K, Tanihata I. Delay-line PPAC for high-energy light ions. *Nucl Instrum Methods Phys Res Sect A* (2001) 470:562–70. doi:10.1016/S0168-9002(01)00804-X

35. Artemov KP, Belyanin OP, Vetoshkin AL, Wolski R, Golovkov MS, Goldberg VZ, et al. Effective method of study of α-cluster states. *Sov J Nucl Phys* (1990) 52:408.

36. Ziegler JF, Ziegler M, Biersack J. Srim – the stopping and range of ions in matter. *Nucl Instrum Methods Phys Res Sect B* 268 (2010) 1818–23. doi:10.1016/j.nimb.2010.02.091

37. Rolfs CE, Rodney WS. *Cauldrons in the cosmos*. Chicago and London: The University of Chocago Press (1988).

38. Lane AM, Thomas RG. R-matrix theory of nuclear reactions. *Rev Mod Phys* (1958) 30:257–353. doi:10.1103/RevModPhys.30.257

39. Larson N. *A code system for multilevel R-matrix fits to neutron data using bayes' equations*. unpublished: ORNL/TM-9179/R5 (2000).

40. Longland R, Iliadis C, Champagne A, Newton J, Ugalde C, Coc A, et al. Charged-particle thermonuclear reaction rates: I. Monte carlo method and statistical distributions. *Nucl Phys A* (2010) 841:1–30. doi:10.1016/j.nuclphysa.2010.04.008

41. Illiadis C. *Nuclear Physics of stars*. New York: VCH (2007).